Available online at www.sciencedirect.com
SCIENCE DIRECT
Polymer 46 (2005) 2675–2684
polymer
www.elsevier.com/locate/polymer

Structural and morphological development in poly(ethylene-*co*-hexene) and poly(ethylene-*co*-butylene) blends due to the competition between liquid–liquid phase separation and crystallization

Zhigang Wang[a,*], Howard Wang[b], Katsumi Shimizu[c], Jin-Yong Dong[a], Benjamin S. Hsiao[d], Charles C. Han[a,*]

[a]*Key Laboratory of Engineering Plastics, Joint Laboratory of Polymer Science and Materials, Institute of Chemistry, Chinese Academy of Sciences, Beijing, 100080, P. R. China*
[b]*Department of Materials Science and Engineering, Michigan Technological University, Houghton, MI 49931, USA*
[c]*Highthroughput Factory, RIKEN Harima Institute, 1-1-1 Kouto, Mikazuki, Sayo, Hyogo, 679-5148, Japan*
[d]*Department of Chemistry, State University of New York at Stony Brook, Stony Brook, NY 17794, USA*

Received 23 October 2004; received in revised form 30 November 2004; accepted 12 January 2005

Abstract

Isothermal crystallization behavior of poly(ethylene-*co*-hexene) (PEH) and the 50/50 blend (H50) of PEH with amorphous poly(ethylene-*co*-butylene) (PEB) was studied by time-resolved synchrotron simultaneous small-angle X-ray scattering/wide-angle X-ray diffraction (SAXS/WAXD) techniques and optical microscopy (OM). The X-ray study revealed the changes of structural and morphological variables such as the scattering invariant, crystallinity and lamellar long period, et al. In H50, the lamellar morphology was found to be dependent on competition between liquid–liquid phase separation (LLPS) and crystallization. At high temperature, LLPS becomes dominating, resulted in crystallization of PEH with minimal influence of PEB. At low temperature, LLPS is suppressed, PEB component shows obvious influence on PEH crystallization, PEB is thought to be partially included into PEH lamellar stacks and PEH-PEB co-crystallization is unlikely, however, possible. Optical microscopy was used to monitor crystal nucleation and growth rates in PEH and H50, providing complementary information about the effect of temperature on LLPS and crystallization. Real-space lamellar morphologies in PEH and H50 were characterized by atomic force microscopy (AFM), PEH exhibited sheaf-like spherulites while H50 exhibited hedrites. Overall, the competition between LLPS and crystallization in H50 blend influences the structural and morphological development. Controlling the interplay between LLPS and crystallization of PEH/PEB blends, it is possible to control the structure and morphology as practically needed.

Keywords: Phase separation; Crystallization; Polyolefins

1. Introduction

Polyolefins industry represents one of the most important sectors in the plastic industry today, and the importance is increasing due to the properties enhancing through the new catalyst developing and alloying processes. Blending of olefin polymers with different compositions, molecular weights and architectures is an important strategy to optimize the properties and processibility of the final product [1,2]. This is particularly the case for recently developed metallocene based polyolefins.

Although the rationale for blending/alloying is appealing, the practice during specific compounding and manufacturing can be complicated and difficult if some fundamental physical principles related to the blending are not understood. For example, both liquid-liquid phase separation (LLPS) and crystallization can co-exist in the process of polyolefin mixing, and these may generate complicate blend morphologies and uncontrollable properties of the final products. In recent years, a great deal of effort has been made to understand the behavior of macroscopic LLPS in blends of ethylene based polyolefins

* Corresponding authors. Tel./fax: +86 10 62558172.
E-mail addresses: zgwang@iccas.ac.cn (Z. Wang), c.c.han@iccas.ac.cn (C.C. Han).

0032-3861/$ - see front matter © 2005 Elsevier Ltd. All rights reserved.
doi:10.1016/j.polymer.2005.01.060

with various microstructures [3–6]. In our group, a quantitative measure of the phase diagram of the nearly isorefractive blends of statistically random ethylene/hexane (PEH) and ethylene/butene (PEB) copolymers has been demonstrated (Fig. 1) [6], and this turns out to be very useful in the study of the driving forces affecting the morphology of the blends. In the phase diagram of PEH and PEB blends, the blend exhibits an upper critical solution temperature (UCST) at $T_s = 146$ °C and ϕ_c (mass fraction) $= 0.44$ in the melt. PEB represents an amorphous component while PEH represents a crystallizable component in the temperature range for this study (90 °C $< T_c <$ 150 °C). The calculated binodal and spinodal boundaries are shown as solid and dashed lines, respectively, and the dotted line indicates the equilibrium melting temperature, T_m^o, measured by differential scanning calorimetry (DSC), as a function of composition. T_m^o for PEH is about 140 °C, lower than linear polyethylene [6]. A similar UCST phase behavior might exist in blends of other branched polyolefins [7].

It is noticed that most studies dealing with the subject of phase separation in polyolefin blends were carried out in the molten state [5,8]. Relatively fewer experiments were made to address the competing effect of crystallization. Those that did, focused mainly on the compatibility issue of the crystalline states, the event of co-crystallization among chains of varying branching or comonomer units, and the melting point depression [3,8–15]. The morphological characterizations in these studies were carried out solely through quenching of samples from the molten state, not during the in-situ process. The objectives of the present study are thus to investigate the time evolution of structural and morphological variables, including the scattering invariant, crystallinity, lamellar long periods, and crystal sizes in PEH and PEH/PEB (50/50) blend during isothermal crystallization at different temperatures by one step quench from the melt. Several time-resolved techniques such as simultaneous synchrotron small-angle X-ray scattering/wide-angle X-ray diffraction (SAXS/WAXD) and optical microscopy were used to follow the structural and morphological changes in the dimensions from nanometers to microns. The lamellar morphology at the surface of quenched samples after isothermal crystallization was examined by atomic force microscopy for comparison.

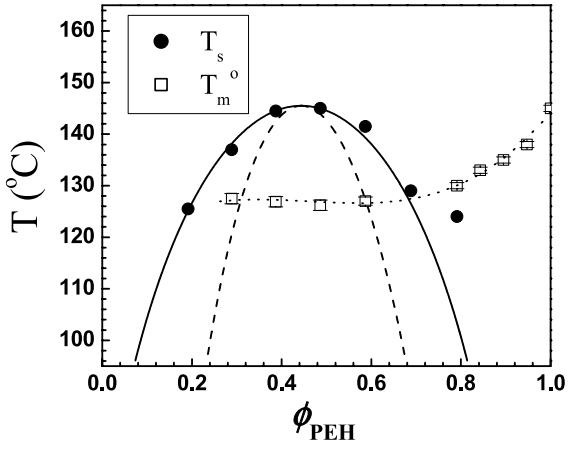

Fig. 1. Phase diagram of PEH/PEB blends. The symbols are measured data points and the solid and dashed curves indicate the calculated binodal and spinodal boundaries, respectively. The dotted line shows the equilibrium melting temperature, T_m^o. The upper critical solution temperature is at $T_c =$ 146 °C and $\phi_c = 0.44$.

Through a comprehensive investigation of evolution of the morphological parameters of PEH and H50 by one step quench from the one-phase melt to crystallization region, the influences of competition between LLPS and crystallization on the structures and morphology can be studied. Because a suitable cross-over temperature of around 118 °C between LLPS and crystallization of H50 [16], H50 can be a beneficial object for this study. Through this study, several questions could possibly be answered, such as whether and how LLPS influences the final lamellar long periods at different crystallization temperature; when crystallization happens, whether PEB involves in the formation of PEH lamellar stacks; if LLPS can be enhanced on purpose, whether it is possible to find out that PEB does entrap in PEH lamellar stacks or PEB even possibly co-crystallizes with PEH; finally, in the one step quench experiment, how many morphological parameters can be adjusted through the competition between LLPS and crystallization. To further illustrate the controlling of structure and morphology, a study of intentionally controlled competition between LLPS and isothermal crystallization by multiple-step quenches will be presented in a future paper.

2. Experimental section

2.1. Samples and preparation

Poly(ethylene-*co*-hexene) (PEH) and poly(ethylene-*co*-butylene) (PEB) were supplied by ExxonMobil Chemical Company. They were statistically randomly copolymers synthesized using a metallocene-catalyst. PEH and PEB had mass-average molecular weights, M_w, of 112 kg/mol and 70 kg/mol, respectively. The corresponding mass densities were 0.922 g/cm^3 and 0.875 g/cm^3, respectively. The branch density ρ was about nine branches per 1000 backbone carbons for PEH and 77 branches per 1000 backbone carbons for PEB. Upon heating, the dried solution-precipitated PEH sample exhibited a T_m of 119.8 °C using DSC at a heating rate of 10 °C/min. For pure PEB, a T_m of 48.6 °C was measured from the dried solution-precipitated sample using a heating rate of 10 °C/min. In this study, PEB was considered as the amorphous component in PEH/PEB blend, because the temperatures used were much higher than the T_m of PEB. The PEH/PEB blend at a composition of 50/50 (by mass and denoted as H50), close to the critical composition in the phase diagram in Fig. 1, was prepared by co-precipitating a hot (about 100 °C) H50/xylene solution into cold (about

0 °C) methanol with a volume ratio of 1–10. After filtration, the blend was first dried in air for 24 h and subsequently dried in a vacuum oven at 100 °C for 72 h. For purposes of comparison, PEH was treated by the same procedure. PEH and H50 films (1 mm thickness) were prepared using a compression molding press (molding temperature 160 °C) between two Kapton films for X-ray measurements.

2.2. SAXS/WAXD

Time-resolved simultaneous synchrotron small-angle X-ray scattering and wide-angle X-ray diffraction measurements, SAXS/WAXD, were performed at the Advanced Polymers Beamline, X27C, in National Synchrotron Light Source (NSLS), Brookhaven National Laboratory (BNL). The wavelength of the X-ray beam was 1.366 Å. The beam size was about 0.4 mm in diameter at the sample position. Synchrotron X-rays were collimated using a three 2° tapered tantalum pinhole collimator [17]. SAXS/WAXD profiles were recorded by two linear position sensitive detectors (European Molecular Biological Laboratory, EMBL), with sample-to-detector distances of 1788 mm for SAXS and 220 mm for WAXD, respectively. The SAXS scattering angle was calibrated with silver behenate and the intensity was normalized by incident beam fluctuations and calibrated with a LUPOLEN standard. The WAXD pixel resolution and the diffraction intensity were calibrated by comparing the synchrotron data with those taken using a Siemens Hi-Star X-ray diffractometer data (Cu Kα) in θ–θ reflection, and were corrected for detector non-linearity and empty beam scattering. The angular scale of the synchrotron WAXD data (λ = 1.366 Å) was also converted to a scale corresponding to λ = 1.542 Å for presentation and discussion.

A dual chamber temperature jump apparatus was used for the isothermal crystallization study. The detailed description of this setup has been reported elsewhere [18]. In this study, the samples were first melted at 160.0 °C (40 °C above the nominal melting point of PEH) for 10 min in one chamber and then pneumatically 'jumped' to the second chamber. This second chamber, aligned in the path of the X-ray beam, was preheated at the desired crystallization temperature for measurement. The true temperature of the sample was measured through a calibrated OMEGA J thermal couple, which was insert to a position near the sample edge (the sample diameter was 0.7 mm). Typical temperature profiles during isothermal crystallization measurement for H50 are shown in Fig. 2, where four representative measurement temperatures are illustrated: 93.8 °C (total measurement time is 16 min), 105.4 °C (60 min), 109.6 °C (42 min) and 114.0 °C (171 min). The different crystallization times used were determined during measurement (the X-ray detection was terminated when the scattering intensity reached a constant value, which is a function of undercooling). In Fig. 2, a fixed time frame of 1000 s is chosen to evaluate the temperature deviation at the early stages of the experiment. It is seen that the transition time to reach temperature equilibrium is between 100 and 160 s. At the equilibrium temperature, the maximum temperature fluctuation was ±0.5 °C. For the PEH sample, the following temperatures were used, 90.5 °C (16.7 min), 98.2 °C (32.7 min), 105.2 °C (32.7 min), 111.5 °C (32.7 min), 113.5 °C (33.3 min) and 117.8 °C (99.3 min). The collection time for each simultaneous SAXS/WAXD profile was 20 s.

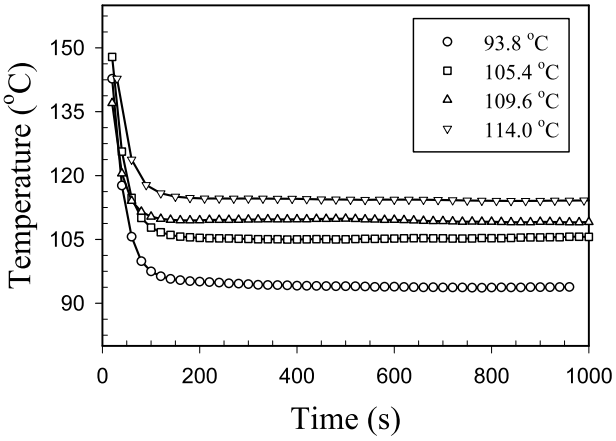

Fig. 2. Time-temperature profiles at the sample position during isothermal crystallization set at four crystallization temperatures.

2.3. Optical microscopy

Nucleation and growth processes of spherulites in PEH and H50 during isothermal crystallization was recorded via bright-field illumination in real-time using a Nikon polarized optical microscope equipped with a Kodak Megaplus CCD camera. Samples of PEH and H50 were hot-pressed between two glass plates at 160 °C to form films with thickness about 20 μm. Crystallization conditions used were similar to those in X-ray measurements.

2.4. AFM

PEH and H50 samples were first prepared by melt-pressing between two clean silicon wafers. One wafer was subsequently removed after quenching the sample to room temperature. Isothermal crystallization studies of PEH and H50 samples were carried out using a heating stage for different periods of time determined from X-ray measurements. The final morphology was preserved by directly quenching of the crystallized sample into ice water. A Dimension™ 3100 AFM (from Digital Instruments) instrument was used to investigate the lamellar morphology on the sample surface. The measurements were carried out in the tapping mode. Both height and phase modes were recorded simultaneously using the retrace signal, with the former providing topological information and the latter providing phase contrast in mechanical properties that

differentiates the crystalline phase from the amorphous phase. In this paper, only phase contrast images will be presented to illustrate different surface morphologies between PEH and H50.

3. Results and discussion

3.1. SAXS/WAXD

Fig. 3 shows typical time-resolved (a) Lorentz-corrected SAXS intensity profiles (Iq^2 versus scattering momentum q ($=4\pi/\lambda*\sin(\theta)$, 2θ is scattering angle)), and (b) WAXD intensity profiles of H50, developed during crystallization at 114.0 °C. During the isothermal crystallization period ($300\ s \geq t \geq 100$ s), the SAXS profile indicates a completely disordered structure of the undercooled melt. The scattered intensity first exhibits a small maximum at $q \approx 0.018$ Å^{-1} at 300 s. The intensity of this peak grows rapidly until it reaches a plateau value. The occurrence of the SAXS peak can be attributed to the formation of lamellar stack structure in PEH crystals, which was verified by AFM and will be shown later. In Fig. 3(b), the corresponding WAXD profiles in the initial isothermal period show only a diffuse amorphous background. The evolution of an orthorhombic unit cell from PEH crystals can be followed through the development of the {110} and {200} reflections. The intensities of these two crystal reflections are found to increase rapidly during the early stages of crystallization and remain almost constant during the late stages of crystallization. The increase of the WAXD intensity from each reflection with time is about the same as that of the SAXS peak.

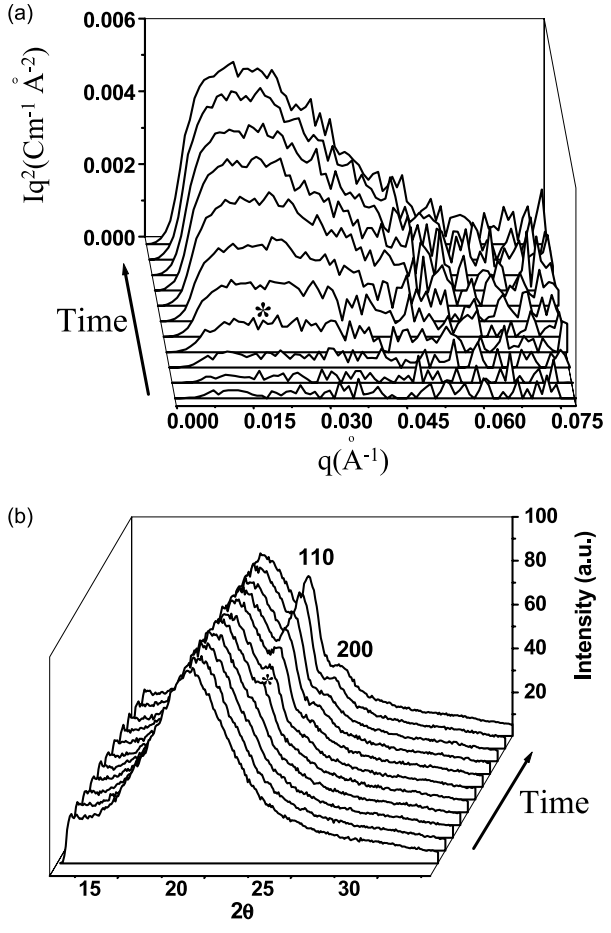

Fig. 3. Typical (a) SAXS and (b) WAXD time-resolved profiles of H50 during isothermal crystallization at 114 °C. Time interval between adjacent profiles is 60 s and the first profile corresponds to 120 s.

In the analysis of SAXS data, the scattering invariant, Q, was calculated by integrating the Lorentz-correct intensity (Iq^2) with q from the beam stop position (about 0.005 Å^{-1}) to 0.08 Å^{-1} (beyond this q position, the scattering only shows statistical noise). Long period, L ($=2\pi/q_{max}$, with q_{max} being the value at the SAXS peak) was determined using Bragg's law. From WAXD data, mass fraction of the crystal phase (X_c) was estimated. The details of above procedures can be found in a previous publication [19]. Fig. 4(a) and (b) illustrate the time evolution profiles of Q (from SAXS) and Xc (from WAXD) of H50 at different temperatures (the value of Xc in Fig. 4(b) has been normalized by the content of PEH component). It is seen that both the scattering invariant (Q) and crystallinity (Xc) exhibit a typical S-shaped growth curve. The solid curves represent the fitted results using a Weibull function [20] to enhance visual trend of the changes. A parameter denoted as 't_c' is defined from the onset point between the initial growth and the extension from the 'plateau' range (marked by an arrow in Fig. 4(b)). The value of t_c, is proportional to half-time of crystallization, indicating crystallization rate [19].

Fig. 4(c) illustrates the characteristic crystallization time, t_c, determined from both time-resolved Q and Xc plots at different temperatures for PEH and H50. At temperatures lower than 110 °C, both PEH and H50 exhibit similar values of t_c and thus similar crystallization rates, indicating that crystallization occurs so fast that SAXS/WAXD can not discern crystallization rates between PEH and H50. At temperatures higher than 110 °C, H50 shows larger values of t_c and slower crystallization rates than PEH. This implies that PEH and PEB components are either not in a deep unstable (spinodal) LLPS region, or with a small (in absolute value) inter-diffusion coefficient (or may be called 'partially miscible' by an in-precise language) and may experience only limited LLPS. This is consistent with the results from a separate kinetics study of PEH/PEB blends by us [16]. In a similar study, reduced polypropylene (PP) spherulite growth rates have been observed in PP/PB1 (poly(butene-1)) blends because of the partial miscibility [21]. In contrast, the growth rate of syndiotactic PP (sPP) spherulites was found to be unchanged in sPP blends with PP of other tacticity (atactic and isotactic), indicating that the melt miscibility is relatively small (or the blends are in a

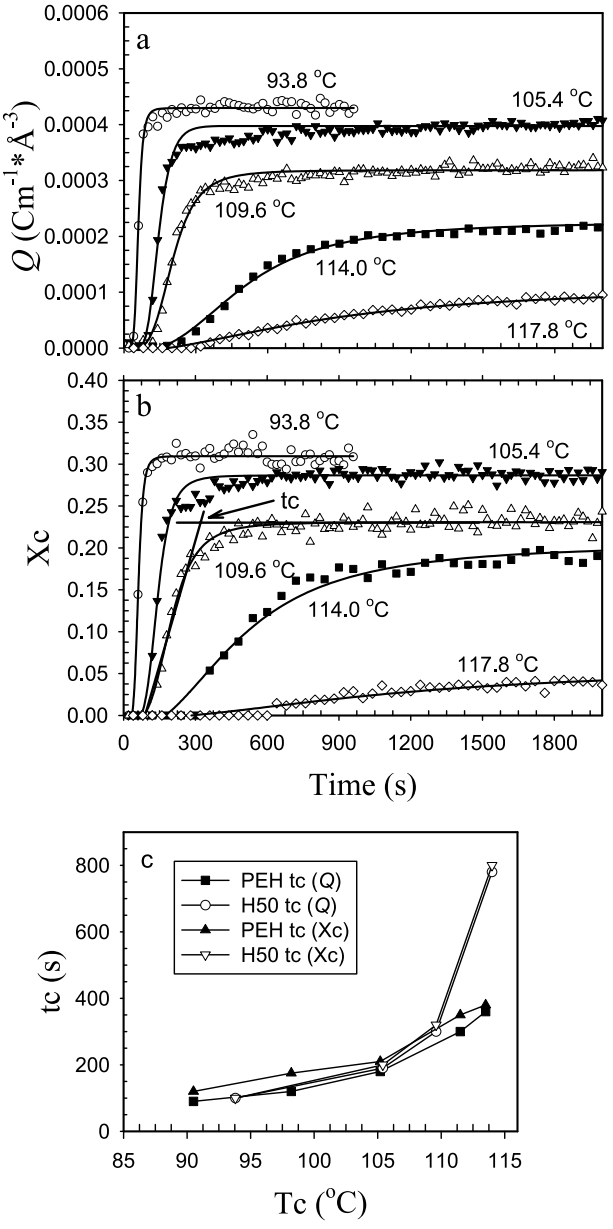

Fig. 4. (a) The scattering invariant of SAXS, Q, and (b) WAXD crystallinity, Xc, versus time at different temperatures for H50; (c) the characterization crystallization time t_c versus crystallization temperature for PEH and H50.

deep quenched LLPS region) between polypropylene isomers [22–23].

Fig. 5 shows the time evolution of lamellar long period, L, in PEH and H50 at different temperatures. It is interesting to observe that there are two opposite trends regarding to the long period changes in both PEH and H50. At low temperatures, long period is found to decrease with time; while at high temperatures, long period increases with time. For PEH, the increase is seen at 117.8 °C; for H50, the increase is seen at much lower temperatures such as 109.6 and 114.0 °C. The sample temperature corresponding to each measured long period is plotted as open symbols in

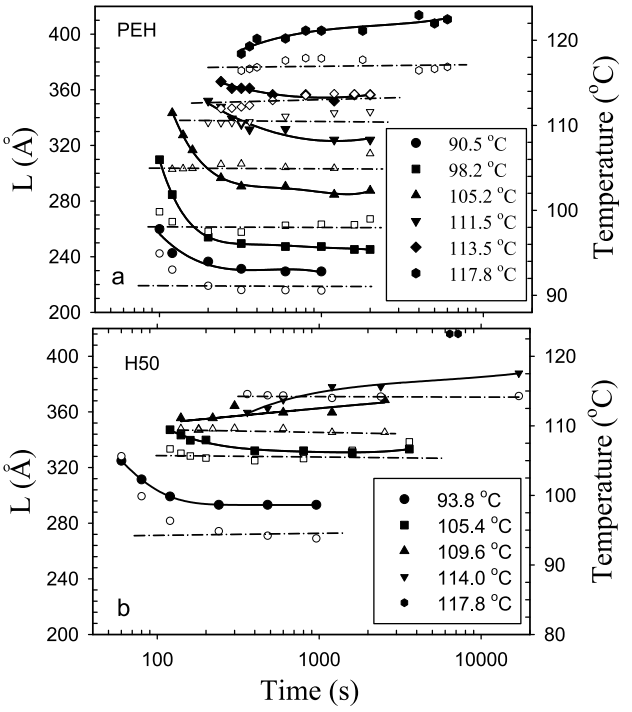

Fig. 5. Lamellar long period, L (filled symbols) versus time at different temperatures for PEH (a) and H50 (b). The open symbols represent the sample temperature corresponding to each long period and the dash line represents the targeted crystallization temperature.

Fig. 5. At temperatures below 100 °C, the long period decrease in the early stage is consistent to the sample temperature dropping for both PEH and H50, because crystallization from melt occurs so rapidly and the sample temperature has not reached the preset temperature. However, the decreases in long period are also observed at 111.5 and 105.2 °C in PEH, and at 105.4 °C in H50, in which the isothermal crystallization temperature has been achieved during measurement. Thus, the long period decrease in the early stages at these crystallization temperatures cannot be explained only by the temperature decreasing. There are two possible explanations for this phenomenon. (1) The continuing formation of thinner lamellar stacks can result in a large decrease of the average long period. This mechanism has been proposed for other semi-crystalline polymers, such as in PBT, [24] PET, [25] nylon 66, [26] and is often referred to as the dual lamellar stacks insertion model [27]. The thinner lamellar stacks are formed because of the reduced entropy in the amorphous regions 'restrained' by the primary lamellar stacks. In Fig. 5, a significant long period decrease is seen in the primary crystallization stage (below t_c). (2) Fractionation occurs during crystallization. That is, the most readily crystallizable chains crystallize first, thereby enriching the remaining melt in more poorly crystallizable chains (shorter or more defective chains). Based on Flory's equilibrium model, at a given crystallization temperature T_c, only the fraction of ethylene sequences with a length greater than the

critical value, $\xi^*(T_c)$, can participate in the crystallization process. This critical value decreases with decreasing T_c. It is then conceivable that the longer ethylene sequences with lower branched chains can form thick lamellae first during the initial nucleation and growth stages, whereas the shorter ethylene sequences with higher branched chains may crystallize later and form thinner lamellae. As a result, the average long period also decreases with time. It is our opinion that both scenarios can exist and the techniques we currently employed cannot distinguish the dominant cause from the other one.

In Fig. 5, the long period increase at higher temperatures can be found and may be due to the lamellar thickening, which has been seen in other polyolefins such as polyethylene, long-chain alkane and homogeneous copolymer of ethylene and 1-octene [28–31]. Lamellar thickening is an inherent consequence of chain-folding crystallization of long chain molecules. Although the folding process provides the fastest mode of crystal growth for linear polymer, it usually leaves the system in a metastable state containing higher surface energy. If the chain possesses sufficient mobility in the crystal, lamellar thickening can take place, which will lower the total free energy. The thickening can occur during isothermal annealing or heating process [30]. Generally, isothermal thickening is a gradual process, with both thickening rate and the final thickness increased by crystallization temperature. This is the main reason that lamellar thickening and long period increasing can be observed at higher crystallization temperature for PEH and H50. It is also interesting to observe that the lamellar thickening in H50 occurs at a much lower temperature than PEH, which indicates higher chain segment mobility of the ethylene crystals in H50 than PEH.

After prolonged isothermal crystallization ($t \gg t_c$), final values of the average lamellar long period, L^*, integrated scattering intensity (or the scattering invariant), Q^* and crystallinity, Xc^*, are obtained and plotted as a function of isothermal crystallization temperature, T_c, in Fig. 6. Within the experimental temperature range, both values of L^* of PEH and H50 increase with increasing T_c. L^* of H50 is found to be higher than PEH and the difference becomes less significant with increasing T_c. In our early study, LLPS was found to be dominating at temperatures above 118 °C (a critical value) for H50. The occurrence of LLPS at higher temperatures creates PEH-rich regions and the crystallization from these regions are similar to PEH, therefore, the finding that the difference in L^* between PEH and H50 reduces with increasing T_c is quite reasonable.

The integrated Lorentz-corrected intensity, Q^*, as a function of T_c in Fig. 6(b), shows two unique features. First, at high temperatures (>115 °C), Q^* exhibits small values, related to low crystallinity due to low degrees of undercooling and slow crystallization rate. Q^* increases rapidly when T_c decreases from 115 to 100 °C, indicating rapidly increasing crystallinity. With further decreasing T_c, Q^* reaches a plateau value for both PEH and H50, indicating

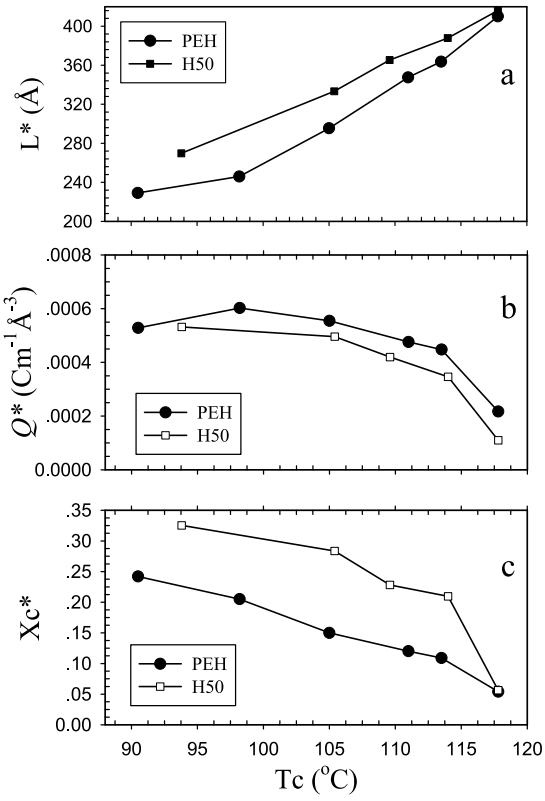

Fig. 6. Final lamellar long period, L^* (a), the final scattering invariant, Q^* (b) and WAXD crystallinity, Xc^* (c) versus T_c for PEH and H50.

almost constant density contrast between the amorphous and crystal phases due to the rapid completion of crystallization and volume filling-up by crystals.

Second, Q^* in H50 at the highest experimental temperature (117.8 °C) is about half of that in PEH. With decreasing temperature, the difference of Q^* between H50 and PEH becomes less and less. In other words, Q^* in H50 is much higher that half of Q^* in PEH at lower temperatures. At the lowest temperatures, Q^* in H50 and PEH becomes even closer. If H50 forms PEH lamellar stacks only composing of PEH crystal lamellar and amorphous layers, and PEH lamellar stacks are viewed as suspended in a PEB amorphous 'lake', which means that PEB has been totally excluded or phase separated from the PEH lamellar stacks, it is predicted that Q^* in H50 shall be appropriately half of PEH [23]. On the contrary, if PEB is included into the amorphous layer within PEH lamellar stacks, Q^* shall have an obvious increase [23]. Thus, changes of Q^* with temperature in Fig. 6(b) clearly indicate that PEB component is involved in the PEH lamellar formation during crystallization at the low temperature ranges. The lower the temperature, the more significant the PEB inclusion into PEH lamellar stacks, due to the more rapid crystallization and more suppressed LLPS. The PEB inclusion is consistent to the increasing long period difference between H50 and PEH with decreasing T_c as shown in Fig. 6(a).

Crystallinity, Xc^*, as a function of T_c in PEH and H50, is shown in Fig. 6(c). For PEH, Xc^* is found to increase almost linearly with decreasing T_c. The composition normalized crystallinity, Xc^*, of H50 is found to have a much higher value than PEH. This experimental result is particularly interesting and unexpected because the normalized crystallinity of H50 is usually thought to be close to PEH. Higher crystallinity of H50 than PEH measured by WAXD might be interpreted as the results of slower crystallization rate, longer crystallization time, larger long periods (larger lamellar thickness) and co-crystallization (that is PEB is partially entrapped inside PEH lamellar stacks) for H50 than PEH. It has been indicated from the dependence of the scattering invariant Q^* and lamellar long period on crystallization time and temperature that PEB component could have been included into the PEH lamellar stacks when crystallization occurs at low temperatures. Furthermore, in this case, although unlikely, but it is possible that some partial chain segments of PEB might participate into the final chain-folding lamellae of PEH. When PEB involves into formation of the lamellar stacks, ordinary composition normalization obviously makes crystallinity much higher. However, further well-controlled experiments need to be designed to prove or reject this co-crystallization possibility.

3.2. Optical microscopy

Comparing to the morphological parameters obtained from reciprocal space by the scattering method, it is useful to investigate the morphology in real space. Nucleation and growth of the spherulites in PEH and H50 were observed by time-resolved optical microscopy. Fig. 7 shows typical micrographs collected during isothermal crystallization of PEH at 118 °C (Fig. 7(a)) and H50 at 114 °C (Fig. 7(b)). In Fig. 7(a), at about 16 min, the nuclei of PEH crystals can be identified. The corresponding crystal growth rate is relatively slow. Even after 122 min of crystallization, PEH crystals still could not fill up the sample space, leaving large fractions of the amorphous 'lake' behind. The spherulites developed during this period are sheaf-like (the general spherical shape is not seen), which are usually observed only in the early stages of polymer crystallization. In PEH, the sheaf-like spherulites are seen even in the very late stages of crystallization at this high temperature.

In Fig. 7(b), nuclei of H50 are observed after 1 min at 114 °C. The spherulites of H50 develop faster than PEH (Fig. 7(a)) because of lower T_c for H50. In Fig. 7(a), sheaf-like spherulites are observed in PEH, while morphology of H50 (Fig. 7(b)) is not so apparent. Upon close examination, the spherulites of H50 are not truly sheaf-like; they branch out more and may be better described as hedrites [32], as shown later by AFM observation. From time-resolved micrographs, the average size of the crystals as a function of time at different temperatures for both PEH and H50 is shown in Fig. 7(c). It is clear that the crystal growth is linear with time for both PEH and H50 prior to the spherulite or hedrite impingements. At the same temperature, H50 shows a slower crystal growth rate than PEH, which is consistent to the SAXS/WAXD results (Fig. 4(c)). Fig. 7(d) shows the crystal growth rates of PEH and H50 at four temperatures. For temperatures lower than 112 °C, optical microscopy does not have enough resolution to track the crystal growth. With increasing T_c, the difference of growth rates between PEH and H50 becomes less. At the highest T_c (118 °C), the growth rates of PEH and H50 become close. This behavior has been explained before. At low temperatures, as crystallization dominates in H50, the miscible PEB component can significantly retard PEH crystallization rate. At high temperature, when crystallization rate is slow and LLPS becomes dominating, the crystal growth rate in PEH-enriched phase becomes less affected by PEB, resulting in close crystallization rates of H50 to PEH.

3.3. AFM

To confirm the lamellar structures extracted by SAXS in reciprocal space, it is useful to observe the morphology of PEH and H50 at high resolution in real space. For this purpose, AFM was applied. Fig. 8 shows typical AFM phase contrast micrographs of PEH and H50 surfaces after having isothermally crystallized for a certain time. In Fig. 8(a), a sheaf-like spherulite in PEH formed at 114 °C for 30 min is seen. The sheaf-like spherulite consists of two lobes of lamellar stacks branching out from the spherulite center, corresponding to SAXS peak shown in Fig. 3(a). Ring-banded structures surrounding the sheaf-like spherulite are observed when quenched into ice water. At high temperature (Fig. 8(b), 118 °C for 120 min), small spherulites are seen, probably due to slow crystallization rate and limited crystallization time; one lobe of the sheaf-like structure is detected by AFM, and another lobe is probably hidden beneath the surface. Fig. 8(c) represents a higher magnification of this sheaf-like structure, with regularly stacked lamellae. The extending, branching and growing of the lamellae seem to occur only within the lobe region (limited to the top side). Upon quenching, small 'fibril-like' lamellae with thinner crystal thickness are formed around the sheaf-like spherulite.

Morphologies of H50 surface after being isothermally crystallized at 114 °C for 117 min and 118 °C for 120 min, respectively, are shown in Fig. 8(d)–(f). Different from PEH, hedrites are formed at 114 °C in H50 (Fig. 8(d)) [32]. The sizes of hedrites in H50 are smaller than those in PEH at 114 °C, consistent with the optical microscopy observation of Fig. 7(c). From phase diagram of PEH/PEB blends, the degree of undercooling is higher for PEH than H50 at the crystallization temperature, so the sizes of crystals in PEH are predicted to be smaller than H50, however, this prediction is not verified. On the contrary, larger crystals are found in PEH than H50. Again, LLPS plays a key role because LLPS of H50 could constrain crystallization within the phase separation domains. Of course, this occurs at

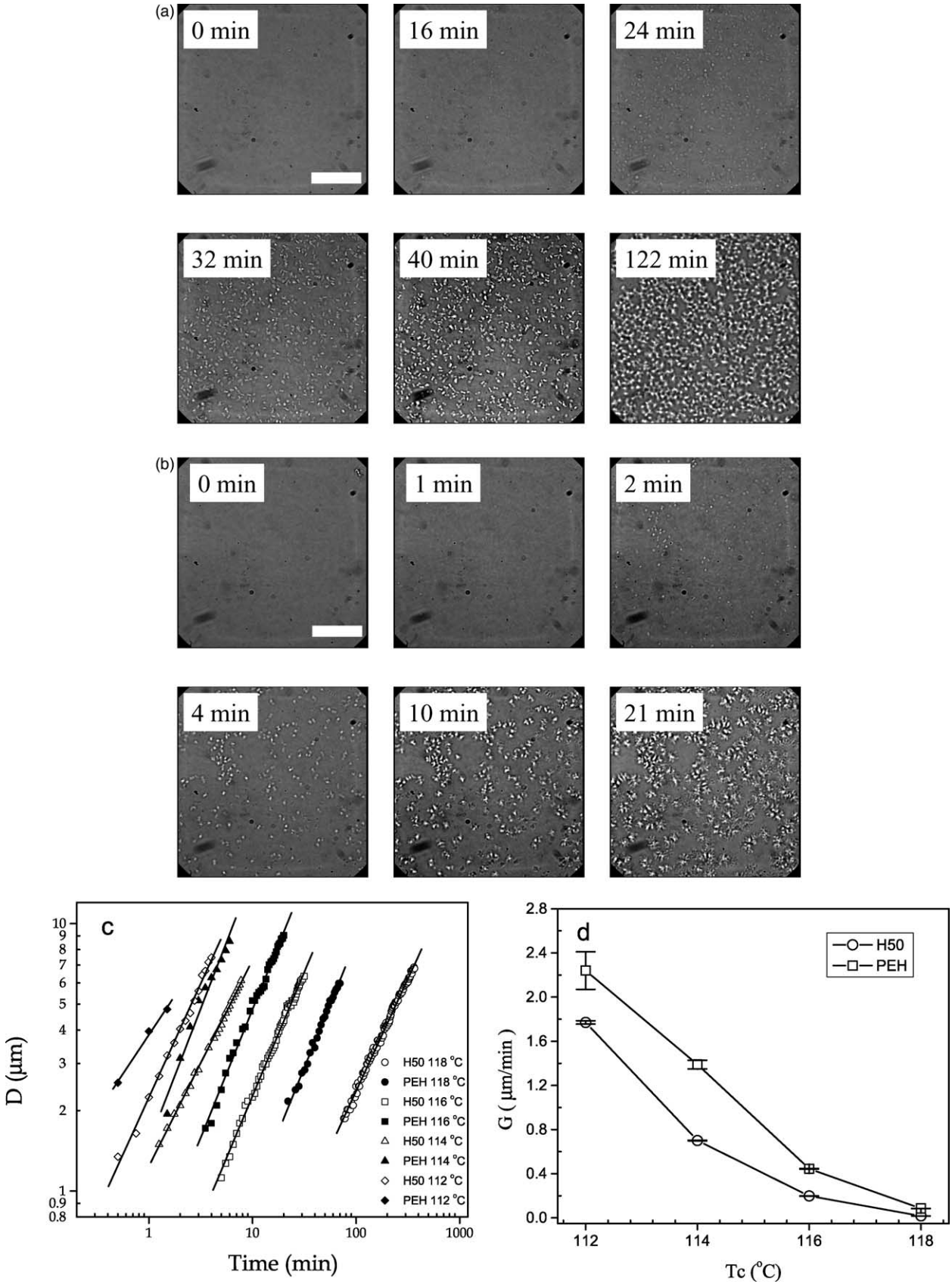

Fig. 7. Serial optical micrographs of PEH at 118 °C (a) and H50 at 114 °C (b) during isothermal crystallization; the crystal sizes versus time at different T_c (c) and the crystal growth rates versus T_c (d) for PEH and H50. The scale bars in (a) and (b) correspond to 40 μm.

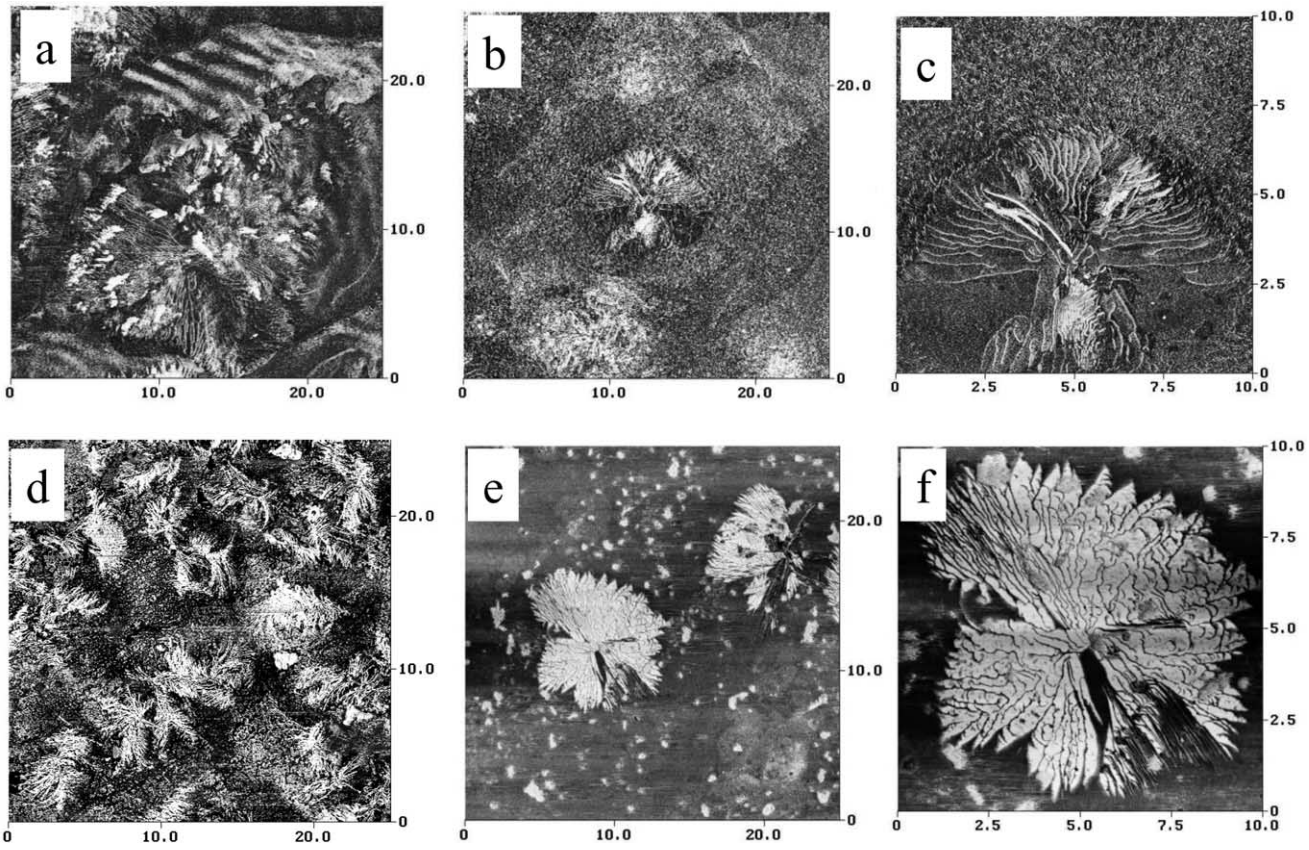

Fig. 8. AFM micrographs of PEH isothermally crystallized at 114 °C (a); at 118 °C (b and c); of H50 isothermally crystallized at 114 °C (d); and at 118 °C (e and f). The scale unit in each micrograph is μm.

relatively high temperatures. At a temperature of 118 °C, hedrites with coarse surfaces are observed (Fig. 8(e) and (f)), indicating that PEB species in H50 do affect PEH crystal growth fronts.

4. Conclusions

One step quench isothermal crystallization behaviors in PEH/PEB (50/50) blend and PEH have been investigated by time-resolved SAXS/WAXD measurement and optical microscopy. The final morphology after isothermal crystallization has been observed by AFM. Time evolution of the SAXS invariant, WAXD crystallinity, lamellar long period and crystal sizes in H50 and PEH are compared. During isothermal crystallization, the lamellar stack insertion and/or fractionation crystallization and lamellar thickening are all observed. The latter is obvious at high temperature. Competition of LLPS and crystallization, depending on the temperature, affects the structural and morphological development in H50 during isothermal crystallization. At high temperature, where LLPS dominates and crystallization rate is slow, PEB component shows less effect on the crystallization behavior of PEH component. At low temperature, LLPS is suppressed and crystallization rate is high, PEB component shows obvious influences on crystallization of PEH component and PEB partial inclusion into PEH lamellae and/or PEB-PEH cocrystallization is possible. Slower crystallization rate, larger long period and larger crystallinity are observed in H50 than PEH. The sheaf-like spherulites and hedrites, with lamellar structures, were observed for PEH and H50, respectively. Optical microscopy shows that the spherulites cannot fill up the whole sample space at a long time scale due to the critical crystallizable chain segment length of PEH component at high temperatures, which is consistent to the SAXS/WAXD measurements. Overall, competition of LLPS and crystallization in H50 blend at one step quench from the melt can be studied due to a suitable cross-over temperature of around 118 °C between LLPS and crystallization and this competition can influence the scattering invariant, crystallinity, lamellar long period, crystallization rate, and the crystal sizes.

Acknowledgements

We acknowledge Dr David J. Lohse of ExxonMobil for providing the samples for this study, and Dr Freddy Khoury of NIST and Professor Jerold Schultz of University of

Delaware for valuable discussion and suggestion. ZW acknowledges the financial support from 'One Hundred Young Talents' of the Chinese Academy of Sciences, P. R. China and the National Science Foundation of China (Grant number 10590355).

References

[1] Paul DR, Newman S. Polymer blends. New York: Academic Press, Inc.; 1978.
[2] Utracki LA. Polymer alloys and blends. New York: Hanser Publishers; 1989.
[3] Crist B, Hill MJ. J Polym Sci: Polym Phys 1997;35:2329.
[4] Mandelkern L, Alamo RG, Wignall GD, Stehlin EC. Trends Polym Sci 1996;4:377.
[5] Hill MJ, Barham PJ. Polymer 2000;41:1621.
[6] Wang H, Shimizu K, Hobbie EK, Wang ZG, Meredith JC, Karim A, et al. Macromolecules 2002;35:1072.
[7] Go M, Shimizu K, Wang H, Wang ZG, Han CC. Polymer 2003;44:7459.
[8] Tanem BS, Stori A. Polymer 2001;42:4309.
[9] Alamo RG, Glaser RH, Mandelkern L. J Polym Sci: Polym Phys 1988;26:2169.
[10] Morgan RL, Hill MJ, Barham PJ. Polymer 1999;40:337.
[11] Li J, Shanks RA, Olley RH, Greenway GR. Polymer 2001;42:7685.
[12] Wignall GD, Alamo RG, Londono JD, Mandelkern L, Kim MH, Lin JS, et al. Macromolecules 2000;33:551.
[13] Alamo RG, Viers BD, Mandelkern L. Macromolecules 1993;26:5740.
[14] Thomann Y, Suhm J, Thomann R, Bar G, Maier RD, Mulhaupt R. Macromolecules 1998;31:5441.
[15] Chen HY, Chum SP, Hiltner A, Baer E. J Polym Sci: Polym Phys 2001;39:1578.
[16] Wang H, Shimizu K, Kim H, Hobbie EK, Wang ZG, Han CC. J Chem Phys 2002;116:7311.
[17] Chu B, Harney PJ, Li Y, Yeh F, Hsiao BS. Rev Sci Instrum 1994;65:597.
[18] Song HH, Wu DQ, Chu B, Satkowski M, Stein RS, Phillips JC. Macromolecules 1990;23:2380.
[19] Wang ZG, Hsiao BS, Sirota EB, Agarwal P, Srinivas S. Macromolecules 2000;33:978.
[20] Mendenhall W, Sincich T. Statistics for engineering and the sciences. 4th ed. Englewood Cliffs, NJ: Prentice Hall; 1995.
[21] Thomann R, Kressler J, Rudolf B, Mulhaupt R. Polymer 1996;37:2635.
[22] Wang ZG, Phillips RA, Hsiao BS. J Polym Sci: Polym Phys 2001;39:1876.
[23] Wang ZG, Phillips RA, Hsiao BS. J Polym Sci: Polym Phys 2000;38:2580–90.
[24] Hsiao BS, Wang ZG, Yeh F, Gao Y, Sheth KC. Polymer 1999;40:3515.
[25] Wang ZG, Hsiao BS, Sauer BB, Kampert WG. Polymer 1999;40:4615.
[26] Wang ZG, Hsiao BS, Murthy NS. J Appl Cryst 2000;33:690.
[27] Verma RK, Hsiao BS. Trends Polym Sci 1996;4:312.
[28] Statton WO, Geil PH. J Appl Polym Sci 1960;3:357.
[29] Fischer EW, Schmidt GF. Angew Chem 1962;74:551.
[30] Anderson FR. J Appl Phys 1964;35:64.
[31] Peterlin A. Macromol Chem 1964;74:107.
[32] Geil PH. Polymer single crystals. New York: Wiley-Interscience; 1963. Chapter 3.